AN H-ADAPTIVE SOLUTION OF THE SPHERICAL BLAST WAVE PROBLEM

Ríos Rodriguez, Gustavo A., Storti M.A, Nigro N.M.
Centro Internacional de Métodos Computacionales en Ingeniería CIMEC
Universidad Nacional del Litoral, CONICET
Güemes 3450, 3000, Santa Fe, Argentina
e-mail gusadrr@yahoo.com.ar

June 25, 2010

Abstract

Shock waves and contact discontinuities usually appear in compressible flows, requiring a fine mesh in order to achieve an acceptable accuracy of the numerical solution. The usage of a mesh adaptation strategy is convenient as uniform refinement of the whole mesh becomes prohibitive in three-dimensional problems. An unsteady h-adaptive strategy for unstructured finite element meshes is introduced. The non- conformity of the refined mesh and a bounded decrease in the geometrical quality of the elements are some features of the refinement algorithm. A three-dimensional extension of the well known refinement constraint for two-dimensional meshes is used to enforce a smooth size transition among neighbour elements with different levels of refinement. A density-based gradient indicator is used to track discontinuities. The solution procedure is partially parallelized, i.e: the inviscid flow equations are solved in parallel with a streamline upwind Petrov-Galerkin finite element formulation with shock capturing terms while the adaptation of the mesh is sequentially performed. Results are presented for a spherical blast wave driven by a point-like explosion with an initial pressure jump of 10^5 atmospheres. The adapted solution is compared to that computed on a fixed mesh. Also, results provided by the theory of self-similar solutions are considered for the analysis. In this particular problem, adapting the mesh to the solution accounts for approximately 4% of the total simulation time and the refinement algorithm scales almost linearly with the size of the problem.

keywords: Mesh adaptation, unstructured grids, hanging nodes, refinement constraints, blast waves.

1   Introduction

Transonic and supersonic inviscid flow problems are common candidates for being adaptively solved because discontinuities usually develop in very thin regions compared to some characteristic length of the problem. The adaptation of the mesh allows to reduce the computational effort required to solve the numeric problem since smaller elements are introduced only where they are needed. In this work, a mesh enrichment procedure based on elements subdivision is introduced for unstructured linear tetrahedra finite element meshes. A desirable feature of any adaptation method is to minimize the geometrical quality degradation of the mesh. The refinement scheme used in this work has shown, through a series of numerical experiments [Ríos Rodriguez et al., 2009], to produce high quality elements without incurring high computational costs. Hanging nodes appear in the refined mesh because no transition elements are used to match zones with differente levels of refinement.

The adaptation stage is sequentially performed while the solution of the Euler equations is computed in parallel using the PETSc-FEM software [Storti et al., 1999-2010]. This latter code uses both a finite element SUPG formulation to stabilize the advective terms of the equations and a shock capturing method for the treatment of shocks [Brooks and Hughes, 1980, 1982, Hughes and Mallet, 1986a,b, Tezduyar and Senga, 2006]. Both stages of the adaptive procedure are coupled through an interface which automates the solution computation. In this way, the boundary conditions for the problem are specified for the starting mesh and are automatically updated. Also, a projected state is given in order to resume the flow computation.

The strategy described in this work is used to solve the spherical blast wave problem driven by a point-like explosion. Besides, the set of ordinary differential equations derived under the Taylor-Sedov self-similar assumptions [Thorne, 2002] are determined. The solutions computed with the adaptive strategy are compared to those obtained on a fixed mesh and also to the self-similar ones.
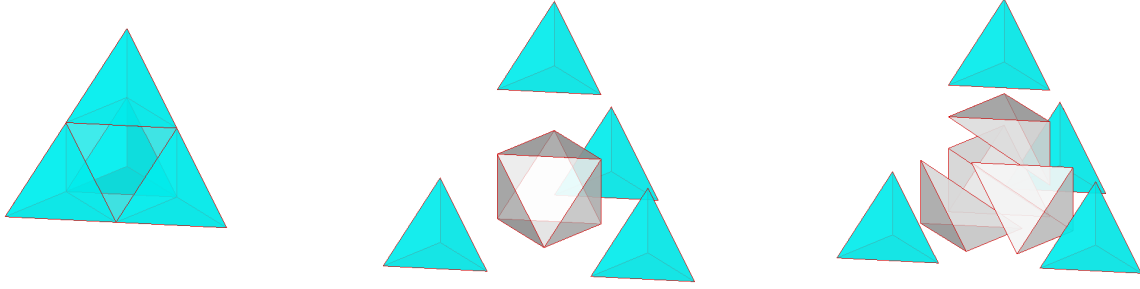
Figure 1: Tetrahedron refinement sequence.

Time measurements of the two main stages in the adaptive solution procedure are realized for analysing the adaptation algorithm from the computational effort point of view as well as its scalability.

2 Refinement schemes and constraints

Since the work of Babuska and Aziz [1976] it is known that the accuracy of the solution in the finite element method strongly depends on the shape of the elements in the mesh. More recently Shewchuck [2002] describes the relationship among the interpolation error, the condition number of the global stiffness matrix in the finite element method and the geometry of the elements. Since refinement procedures usually reduce the quality of the mesh, some care has to be taken when deciding how to refine the elements. The approach taken in this work only applies regular (isotropic) 1:8 subdivision patterns to the elements. However, as no regular 1:8 subdivision exists for tetrahedra, a refinement scheme that shows a good trade-off between the requiered computational effort and the geometrical quality of the resulting tetrahedra is desirable. In Ríos Rodriguez et al. [2009] it is shown through numerical experiments that in most of the cases, refining a tetrahedron by joining the midpoints of its edges and choosing then the shortest diagonal of the inner octaedron (see Fig.1) allows to maximize the minimum value of the quality index for the resulting elements. Also, the successive application of this refinement scheme to the minimum quality element shows that the minimum quality diminishes only in the first refinement and then keeps constant. The geometrical quality of the tetrahedra was measured with both the minimum dihedral angle and the mean ratio shape measure η introduced by Liu and Joe [1994], namely

$$\eta(T) = \frac{12(3V)^{2/3}}{\sum_{i=1...6} l_i^2} \tag{1}$$

where V is the volumen of the tetrahedron T and l_i are the lenghts of its edges.

But besides the shape's quality of the elements, their size distribution also influence the condition number of the stiffness matrix in the finite element method [Shewchuck, 2002]. A smooth change in the size among neighbour elements in the mesh is required in this sense. Because no transition elements are used to match zones with different levels of refinement, some refinement rule must be assumed. We adopt the 1-irregular mesh refinement constraint which was initially proposed in [Babuska and Rheinboldt, 1978] and has been used in many commercial and academic adaptive codes since then [Greaves, 2004, Popinet, 2003, Remacle et al., 2002]. The rule states that *no more than one hanging node should be shared among neighbour elements through the common edge to which the hanging node belongs*.

However, for three-dimensional meshes the neighbourhood among elements through edges and faces as well as the refinement of *orphan* edges on triangular faces have to be considered. In this work, we call orphan edge to that one which is not obtained by the refinement of another edge.

Consider the tetrahedral mesh shown in Fig.(2.a). Assume that the element that "touches" the face defined by the vertices $a - b - c$ with the orphan edge $\overline{n_1 n_2}$ needs to be refined. Figure 2.b) shows how the refined mesh would look like after refinement if the two-dimensional constraint were just considered. It can be seen that a difference of more than one level of refinement would exist among nearby elements in the mesh. To avoid this situation, the strategy developed in this work also refines the element that shares the face $a - b - c$ if at least one of the orphan edges on that face has to be refined. Figure 2.c) shows the refined mesh that is obtained in this latter case.
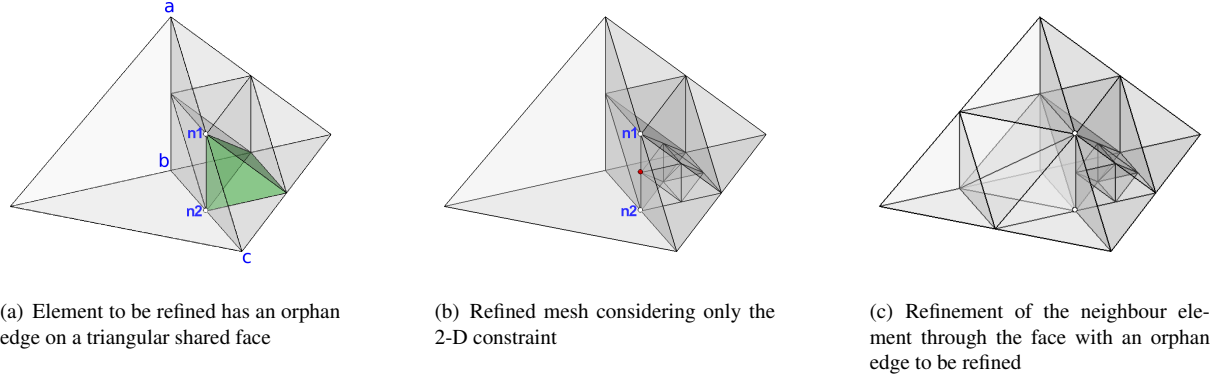
(a) Element to be refined has an orphan edge on a triangular shared face

(b) Refined mesh considering only the 2-D constraint

(c) Refinement of the neighbour element through the face with an orphan edge to be refined

Figure 2: Refinement constraint for 3-D meshes - Orphan edge case.

3   Mesh adaptation strategy

The adaptive solution of the problem begins by solving the Euler equations on a conforming mesh, hereafter called the *base mesh*. After a fixed number of time steps (*nsteps*), the regions of the base mesh that need to be refined are selected. In this work the selection criterion is based on the magnitude of the density gradient computed in an element-wise fashion. All the elements whose gradient magnitude is equal to or greater than a percentage of the maximum gradient for all the elements in the mesh are refined

$$c_1 \leq \frac{\| \nabla_i \rho \| \cdot h_i}{\max_i(\| \nabla_i \rho \| \cdot h_i)} \tag{2}$$

where c_1 is a constant set beforehand by the user, h_i is a measure of the element size and $\| \nabla_i \rho \|$ is the magnitude of the density gradient computed for the element. The accurate choice of c_1 mostly depends on the user's experience.

A succession of nested non-conforming meshes is then generated by applying the refinement rules described in the previous section until a maximum level of refinement is reached. This constraint on the number of refinement levels is applied because in problems where discontinuities in the solution exist, there is no stopping criterion if eq.(2) is used to select the elements to be refined.

It is worth to mention that although the adapted meshes introduce hanging nodes on the edges or faces of an element and assuming that linear finite elements are used, constraining the solution at these hanging nodes to the average at the nodes which define those edges or faces, ensures the solution's continuity among nearby elements.

As the base mesh in refined, the state computed by the solver is linearly interpolated and the boundary conditions are updated. When the maximum level of refinement is attained the interpolated state is used as the initial condition to resume the numerical solution procedure.

After the solution is advanced *nsteps* time steps, the selection criterion given by eq.2 is applied again to the last computed solution and elements are marked to be refined. The adaptation strategy here developed assumes that all the elements that are not selected for refinement should be unrefined up to the base mesh level. Also, since a maximum level of refinement is imposed, only those elements that do not belong to the maximum level of refinement are finally included in the list of elements to be refined. On the other hand, an element is unrefined if only all its *brothers* (7 in three dimensions and 3 in two dimensions) are also marked to be unrefined. If this is so, they are replaced by their *parent* element in the mesh. This *search parent* procedure is recursively applied on the data structure that stores the hierarchical relationship of the elements in the mesh until the base mesh level is attained. It must be taken into account that although some elements are initially marked to be unrefined, the subsequent application of the refinement and unrefinement constraints may not allow it.

A few words about the frequency for the adaptation of the mesh would like to be mentioned, since it is set constant for the whole simulation. First of all, the time step size for the fluid flow problem is updated after every mesh adaptation in order to satisfy the Courant-Friedrich-Lewy (CFL) condition for compressible flows [Laney, 1998] so the time simulated between two successive adaptations of the mesh is not constant. Because the most refined regions of the mesh are expected to be at the discontinuities, the time step size will be dictated by the size of those elements. This helps to prevent the discontinuities to move outside of the most refined regions until the mesh is adapted again.

The proper choice of the adaptation frequency depends on various factors. Several authors [Remacle et al., 2002, Ripley et al., 2004, Waltz, 2004] find in practice that the adaptation of the mesh takes just a small fraction of the overall simulation time (approximately less than 5 per cent). This result induce us to choose a high updating frequency for the mesh for not compromising the overall performance of the adaptive solution procedure. If the time required by the adaptation of the mesh were found to be a greater percentage of the overall simulation time, then a lower updating frequency should be chosen. However, in this latter case a bigger cost would be transferred to the flow computation stage since the refined regions of the mesh would need to be wider to ensure that discontinuities will be kept inside them until the mesh is adapted again. Choosing a higher frequency for adapting the mesh enables to use narrower refined regions around discontinuities and the fluid flow problem is less expensive to solve.

The boundary conditions and other properties applied to the mesh entities are handled by a property identifier or flag associated to the entities of the base mesh. This flag is inherited from a parent entity to its children during the adaptation procedure. The flag is defined by the user and can describe a set of features of different nature for an entity (e.g. the identifier assigned to a face could mean that a slip boundary condition has to be enforced on that face and also that the face belongs to a curved surface which defines a particular section of the boundary). The user must supply a list of vertices which define the entities of the mesh that have a particular set of properties. Then the flag is only assigned to an entity provided certain conditions on the list of vertices are satisfied (e.g. if a set of properties is to be applied to faces then the condition might be that *all* the vertices of the faces should be in the list for the identifier to be assigned). After refinement, the entities with the same properties are identified in order to update the boundary conditions supplied to the flow solver.

4   The spherical blast wave problem

The blast wave problem was formerly and independently studied by Taylor [1946, 1950a,b] and Sedov [1959], and describes what happens if a point-like explosion occurs in a uniform density gas. After a short lapse of time one expects to find a spherical shock wave travelling radially outward at supersonic speeds with a transonic flow behind it. This shock wave comes to an end because the source of pressure (.i.e. the release of energy) also comes to an end. This allows the rarefaction wave generated in the center of the explosion to weaken the spherical shock until it becomes a pressure wave. When this kind of phenomena takes place it is said that a blast wave happens.

4.1   Self-similar solutions

Taylor and Sedov analysis assumes a self-similar solution for the problem, which means that the solution profiles for the density ρ, velocity u and pressure p keep their shape in time and depend only on a single parameter ξ that is defined as the ratio of the radial coordinate r measured from the center of the explosion to the position of the spherical shock front R, so that $0 \leq \xi \leq 1$. Taylor and Sedov formulate the following relationship between the physical variables and the self-similar profiles for the velocity $U(\xi)$, density $\Omega(\xi)$ and pressure $P(\xi)$

$$u = \dot{R}U(\xi), \quad \rho = \rho_0\Omega(\xi), \quad p = \rho_0\dot{R}^2P(\xi) \tag{3}$$

This solution holds as long as the mass swept up by the spherical shock front is much greater than the mass of the explosive material and as long as the shock wave can be considered strong. The equations for the self-similar solutions are derived from the Euler equations in radial coordinates

$$\frac{\partial \rho}{\partial t} + \frac{1}{r^2}\frac{\partial}{\partial r}\left(r^2\rho u\right) = 0 \tag{4}$$

$$\frac{\partial u}{\partial t} + u\frac{\partial u}{\partial r} + \frac{1}{\rho}\frac{\partial p}{\partial r} = 0 \tag{5}$$

$$\frac{\partial p}{\partial t} + u\frac{\partial p}{\partial r} - c_s^2\left(\frac{\partial \rho}{\partial t} + u\frac{\partial \rho}{\partial r}\right) = 0 \tag{6}$$

The latter can be reduced to a system of ordinary differential equations if it is further assumed that the density shows a power law dependence in space and time and the shock front position obeys to a power law in time. The ODE's are then numerically integrated with a fourth order Runge-Kutta method assuming the following boundary conditions inmediately behind the shock front (at $\xi = 1$)
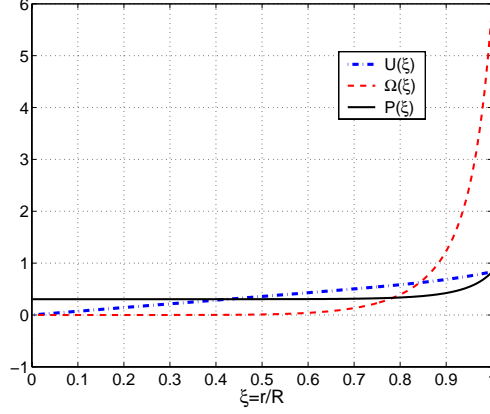
Figure 3: Self-similar profiles for the spherical blast wave problem ($\gamma = 1.4$).

$$U = \frac{2}{\gamma+1}, \quad \Omega = \frac{\gamma+1}{\gamma-1}, \quad P = \frac{2}{\gamma+1} \tag{7}$$

The self-similar computed profiles plotted against the similarity parameter are shown in Fig.(3). It is seen that the pressure in the center of the blast wave is almost half the maximum pressure inmediately behind the shock and it is fairly uniform within the blast wave. It can also be seen that most of the ambient gas mass processed by the shock wave is compressed within a thin spherical shell inmediately behind the shock which moves slightly slower than the shock itself ($u \simeq 0.83\dot{R}$ if $\gamma = 1.4$). Finally the velocity profile is almost linear in the blast wave, with the fluid being at rest in the center of the explosion.

By a simple dimensional analysis it can be found that

$$R(t) \propto \left(\frac{E_x}{\rho_0}\right)^{1/5} t^{2/5} \tag{8}$$

where E_x is the energy released by the explosive material. The constant Q that allows to equate both sides of Eq.(8) can be computed by numerical integration of the total energy profile for a given time instant given by

$$E_x = \int_0^R \left(\frac{p}{\gamma-1} + \frac{\rho u^2}{2}\right) 4\pi r^2 dr \tag{9}$$

Changing to variable ξ and substituting u, p and ρ from Eqs.(3) in the integral of Eq.(9), taking into account that $\dot{R} = \frac{2}{5}\frac{R}{t}$, then replacing E_x given by Eq.(9) into Eq.(8) and finally solving for Q it is found

$$Q = \left(\frac{16\pi}{25} \int_0^1 \left(\frac{P(\xi)}{\gamma-1} + \frac{\Omega(\xi)U(\xi)^2}{2}\right) \xi^2 d\xi\right)^{-1/5} \tag{10}$$

If a value of $\gamma = 1.4$ is assumed, the approximate value for Q is 1.165.

4.2 Finite element solutions

The finite element problem is solved on a spherical domain of radius $R_{ext} = 5$m. Although the problem has spherical symmetry, it is solved as 3-D since one the goals of the simulation, besides verifying if there is an improvement in the shock resolution, is both to evaluate how much of the total computation time is required to adapt 3-D meshes and how the recursive refinement algorithm scales with the size of the problem.

The assumed initial conditions are: the resting ambient gas is air, at a constant pressure and density equal to $p_0 = 101325$Pa and $\rho_0 = 1.225$kg/m^3, and the energy released by the explosive instantly raises the pressure to $p_{blast} = 10^5 \cdot p_0$ in a small spherical region of radius $R_{blast} \simeq 0.25$m. The initial explosion that generates these state is not simulated in the work but it is assumed that it is a constant volume evolution. The pressure fixation at the
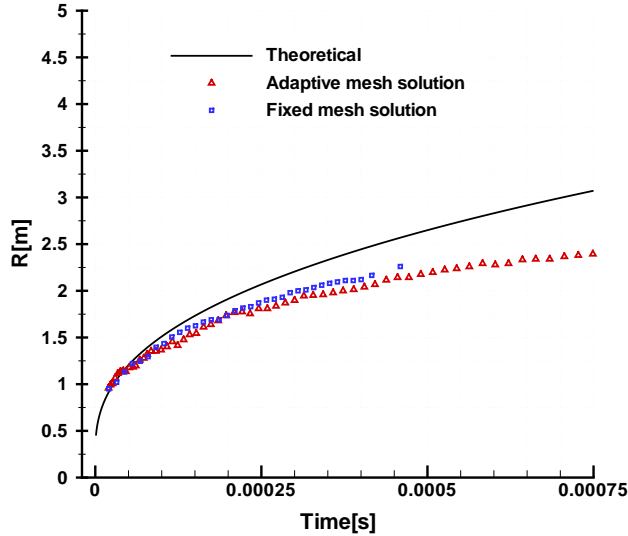
5

Figure 4: Shock wave position as a function of time.

surface of the spherical domain is the only boundary condition prescribed. This condition can be applied as long as the shock wave does not reach the domain's boundary.

Tetrahedral elements are used to subdivide the problem domain with elements of smaller size prescribed towards the center of the sphere. The resulting mesh has 421.000 tetrahedra and 76.500 vertices approximately. This mesh is used as the base mesh for the adaptive simulation and as the fixed mesh for the non-adaptive one.

The Euler equations are solved in parallel with 15 processors on a cluster of workstations and a Backward-Euler scheme is used for time integration. It is recalled that the magnitude of the density gradient is chosen as an indicator for the adaptive simulation since the flow field generated by the blast wave is dominated by a strong shock and an expansion wave. A value of $c_1 \simeq 0.15$ is used in Eq.2 for the simulation. Also, an adapting frequency of 10 time steps is chosen and a maximum of 2 levels of refinement is prescribed. The final time for both simulations is equal to $t_f \simeq 0.001$s.

4.3 Simulation results

In comparing the position of the shock front to that given by Eq.(8) it should be taken into account that the FEM solution profiles will just approximate those of the self-similar ones after a few time steps because the initial conditions for the flow variales are not those of the self-similar profiles from the theory. Bearing this in mind, Fig.(4) shows the shock wave position as a function of time for both the adapted and fixed mesh simulations superposed to the analytical solution given by Eq.(8). It can be stated that although there is a good agreement for the first time instants, both simulations lug behind the analytical one by almost 15% (adaptive) and 14% (non-adaptive) at $t = 0.00045$s.

The Mach number and the logarithm of the pressure along the radius for different time instants are shown in Figs.(5.a) and (5.b), computed with both the adapted mesh and the fixed one. Figure (5.b) shows that the pressure within the blast wave behaves like that predicted by the self-similar solution, that is, it is fairly uniform and has a value that is half the maximum reached immediately behind the shock. The Mach number within the blast wave is depicted in Fig.(5.a) showing that it is in the transonic-subsonic regime in agreement with the theory. Both figures show that the entire flow field is better resolved using the adaptive procedure because no spurious oscillations appear in the expansion region behind the shock wave and the shock front is sharply defined. As a consequence, higher values for the pressure are reached at the shock front and within the blast wave. The shock wave travels roughly at an average speed of 3000m/s at the simulated final time t_f, i.e. it travels at mach number $M_S \simeq 9$, so that the strong shock assumption of the self-similar solutions holds. Figure (6) depicts a cut of the mesh on a plane of symmetry at $t = 0.645$ms. This figure shows that the region of two-level refined elements propagates in a thin region of one-level refined elements because of the refinement constraint. This mesh has approximately 2.34 million tetrahedra and 428000 vertices.
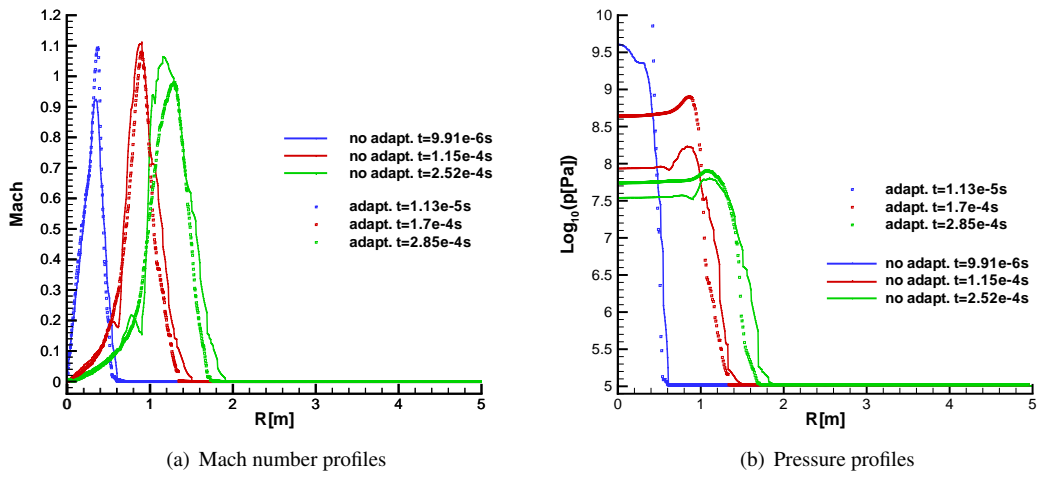
6

(a) Mach number profiles

(b) Pressure profiles

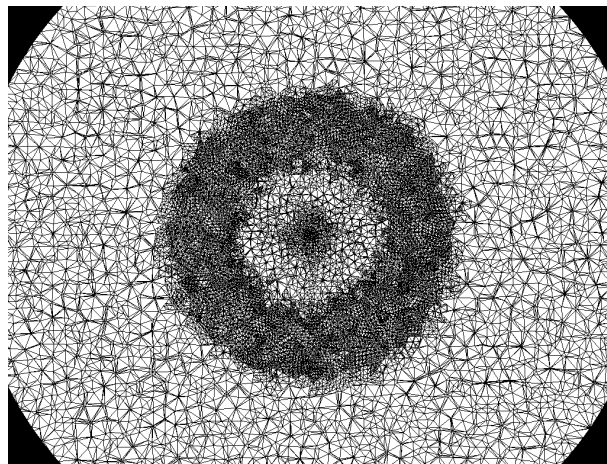Figure 5: Time evolution of the flow field within the blast wave.

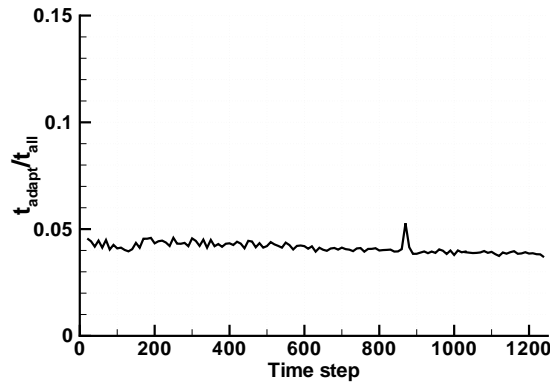Figure 6: Adapted mesh on a plane of symmetry at time $t = 0.645$ms.

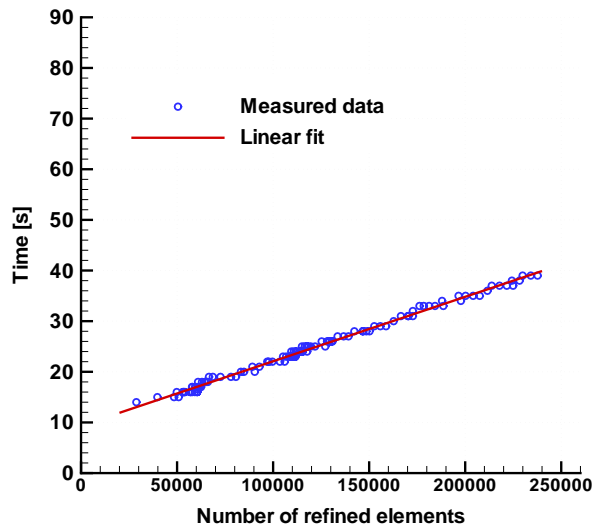Figure 7: Relative cost for the adaptation of the mesh.

Figure 8: Refinement algorithm scalability.

4.4 Mesh adaptation cost

To evaluate the mesh adaptation code performance, clock time to perform the adaptation of the mesh and to compute the equations solution is measured throughout the simulation. The adaptation time t_{adapt} is defined as that required to realize all the necessary tasks to adapt the mesh, namely the error indication computation, the refinement of the elements, the boundary conditions update, the state projection, the time step size update using the CFL condition and the writting to disk of all the files requiered by the flow solver. On the other hand, the solution time t_{sol} takes into account both the time requiered to advance the solution plus the overhead incurred to restart the flow computation. Overall time is then defined as $t_{all} = t_{adapt} + t_{sol}$. Figure (7) shows that the ratio t_{adapt}/t_{all} keeps almost constant and equal to 0.04, which enables to state that, for this particular problem, the adaptation of the mesh takes just a small fraction of the solution time. Given that the biggest effort is involved in the solution of the flow equations, maybe a higher updating frequency for the mesh could have been used.

On the other hand the refinement algorithm scalability is depicted in Fig.(8), where the clock time measured taken by the recursive algorithm of refinement is shown in the ordinates and the refined elements number is shown in abscissa. It is seen that an almost linear scalability is attained, at least for the range of refined elements $50.000 < Nele_{ref} < 240.000$. A linear fit is superimposed in the same picture as a reference.

5 CONCLUSIONS

The mesh adaptation strategy is used to solve the spherical blast wave problem, improving the sharpness of the shock front and removing the spurious oscillations in the expansion which are present in the non-adapted mesh solution. The behaviour of the flow field variables agrees rather well with the theoretical results from the Taylor-Sedov self-similar solution. Although the shock front position is not so accurately predicted this cannot be ascribed to the adaptation of the mesh since the non-adapted solution also shows a similar lack of precision. It is thought that a deeper research of the flow modelling is needed in this sense.

The overhead introduced by the adaptation of the mesh is just a small percentage of the time required to compute the flow, thus allowing to greatly reduce the computational effort. If we were to solve the problem with a fixed mesh to get a similar accuracy (in fact, if each tetrahedron of the base mesh used for the simulations and then all their sons were refined following the 1:8 pattern used by the adaptation procedure) a fixed mesh made up of 26.9 million would have been requiered. So it is concluded that true benefits are achieved because of adapting the mesh, namely an accuracy improvement and a reduction of the computational effort.

Acknowledgments

References

I. Babuska and A.K. Aziz. On the angle condition in the finite element method. *SIAM J.Numer.Anal*, 13:214–226, 1976.

I. Babuska and W.C. Rheinboldt. Error estimates for adaptive finite element computations. *SIAM Journal on Numerical Analysis*, 15(4):736–754, 1978.

A.N. Brooks and T.J.R. Hughes. Streamline Upwind/Petrov Galerkin methods for advection dominated flows. In *Third Internat. Conf. of Finite Element Methods in Fluid Flow*, Banff, Canada, 1980.

A.N. Brooks and T.J.R. Hughes. Streamline Upwind/Petrov Galerkin formulations for convective dominated flows with particular emphasis on the imcompressible Navier-Stokes equations. *Comput. Methods Appl. Mech. Engrg.*, 32:199–259, 1982.

Deborah Greaves. A quadtree adaptive method for simulating fluid flows with moving interfaces. *J. Comput. Phys.*, 194(1):35–56, 2004. ISSN 0021-9991. doi: http://dx.doi.org/10.1016/j.jcp.2003.08.018.

T.J.R. Hughes and M. Mallet. A new finite element formulation for computational fluid dynamics: Iii. The generalized streamline operator for multidimensional advective-diffusive systems. *Comput. Methods Appl. Mech. Engrg.*, 58(3):305–328, 1986a.

T.J.R. Hughes and M. Mallet. A new finite element formulation for computational fluid dynamics: Iv. A discontinuity-capturing operator for multidimensional advective-diffusive systems. *Comput. Methods Appl. Mech. Engrg.*, 58(3):329–336, 1986b.

C. Laney. *Computational Gasdynamics*. Cambridge University Press, 1998.

A. Liu and B. Joe. On the shape of tetrahedra from bisection. *Mathematics of Computation*, 63(207):141–154, July 1994.

S. Popinet. Gerris: a tree-based adaptive solver for the incompressible Euler equations in complex geometries. *Journal of Computational Physics*, 190:572–600, 2003.

J. Remacle, X. Li, N. Chevaugeon, and M.S. Shephard. Transient mesh adaptation using conforming and non conforming mesh modifications. In *Proc. 11th Int. Meshing Roundtable, Sandia*, 2002.

G.A. Ríos Rodriguez, M. Storti, and N.M. Nigro. An h-adaptive unstructured mesh refinement strategy for unsteady problems. *Latin American Applied Research*, 39:137–143, 2009.

R.C. Ripley, F.S. Lien, and M.M. Yovanovich. Adaptive unstructured mesh refinement of supersonic channel flows. *Int. Journal of Comp. Fluid Dynamics*, 18:189–198, February 2004.

L.I. Sedov. *Similarity and Dimensional Methods in Mechanics*. Academic Press, New York, 1959.

J. R. Shewchuck. What is a good linear finite element? interpolation, conditioning, anisotropy and quality measures. URL http://www.cs.berkeley.edu/ jrs/papers/elemj.ps, 2002.

M. Storti, N. Nigro, R. Paz, L. Dalcín, L. Battaglia, E. López, and G.A. Ríos Rodriguez. *PETSc-FEM, A General Purpose, Parallel, Multi-Physics FEM Program*. CIMEC-CONICET-UNL, 1999-2010.

G.I. Taylor. The air wave surrounding an expanding sphere. In *Mathematical and Physical Sciences*, volume 186 of *Series A*, pages 273–292. Royal Society of London, Royal Society, September 1946.

G.I. Taylor. The Formation of a Blast Wave by a Very Intense Explosion. I. Theoretical Discussion. In *Mathematical and Physical Sciences*, volume 201 of *Series A*, pages 159–174. Royal Society of London, Royal Society, March 1950a.

G.I. Taylor. The Formation of a Blast Wave by a Very Intense Explosion. II. The Atomic Explosion of 1945. In *Mathematical and Physical Sciences*, volume 201 of *Series A*, pages 175–186. Royal Society of London, Royal Society, March 1950b.

T.E. Tezduyar and M. Senga. Stabilization and shock-capturing parameters in supg formulation of compressible flows. *Computer Methods in Applied Mechanics and Engineering*, 195:1621–1632, 2006.

Kip Thorne. Applications of classical physics, 2002. www.pma.caltech.edu/Courses/ph136/yr2002.

J. Waltz. Parallel Adaptive Refinement for Unsteady Flow Calculations on 3D Unstructured Grids. *Int. J. Numer. Meth. Fluids*, 46:37–57, 2004.